Energy Conversion and Management 293 (2023) 117444

Contents lists available at ScienceDirect

Energy Conversion and Management

journal homepage: www.elsevier.com/locate/enconman

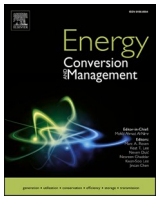

Design and performance assessment of a pumped hydro power energy storage connected to a hybrid system of photovoltaics and wind turbines

Bader Alqahtani [a,b], Jin Yang [a], Manosh C Paul [a,*]

[a] Systems, Power & Energy Research Division, James Watt School of Engineering, University of Glasgow, Glasgow G12 8QQ, United Kingdom
[b] Department of Mechanical Engineering, College of Engineering, University of Bisha, P.O. Box 001, Bisha 61922, Saudi Arabia

ARTICLE INFO

Keywords:
Hybrid renewable energy system
Pumped hydropower energy storage
Solar energy
Wind energy

ABSTRACT

Worldwide, the overdependence on conventional power plants for electricity generation has been one of the most significant economic and environmental challenges. Renewable energy sources have become the most viable option to overcoming this issue. Recently, a hybrid renewable energy system consisting of wind turbines and photovoltaics combined with a pumped hydroelectric energy storage system has received considerable interest. However, neglecting crucial parameters, such as head losses and evaporation rate, might reduce the accuracy of the total simulation performance, resulting in an underestimation of the correct size of each component. This study investigates this issue by proposing a robust approach with a strategy to establish the ideal pipe design through an in-depth techno-economic assessment. A comparative analysis between two different scenarios in which one considers head loss and the other does not is carried out. A wide range of proposed system configurations has been thoroughly investigated. The essential performance indicators employed for designing the proposed system are the renewable energy fraction and the loss of renewable energy, and the results reveal that these two indicators have improved by approximately 8.6% and 3%, respectively. The most significant annual variation between the two scenarios regarding the total demand satisfied by the proposed system and the amount of renewable energy loss is 218.23 GWh and 89.39 GWh, respectively. The pipe efficiency at the pumping and generating modes, which is determined through a sensitivity analysis, ranges between 91-99% and 76–95%, respectively. These findings could assist designers in making initial assumptions about such parameters with reasonable confidence.

1. Introduction

1.1. Background and motivation

The energy sector plays an essential role in most communities by providing the electricity and heat on which most world residents and industries depend. However, conventional power plants, the primary source of electricity, are responsible for meeting the high demand for energy worldwide, resulting in extensive emissions of greenhouse gases [1]. To reduce these harmful emissions, decrease the depletion of non-renewable resources such as oil and natural gas, and address environmental pollution, it is crucial to shift from dependence on conventional fossil-fuel based power to renewable energy sources (RES) such as solar and wind energy [2]. However, RES are still not trustworthy because of fluctuations in natural sources (e.g., wind speed, sun radiation) which can negatively impact grid stability and reduce reliability whether connected to a national grid or a stand-alone system. To deal with this unpredictability, it has been widely recommended in the literature that various sources of renewable energy should be combined as a hybrid renewable energy system (HRES) or that they should be integrated with an appropriate energy storage system (ESS) [3].

1.2. Literature review

The hybridisation of renewable energy sources, such as photovoltaic (PV) systems and wind turbines, as well as EES, such as a battery or pumped hydropower energy storage (PHES), has gained considerable attention in recent years. Singh et al. [4] conducted a study to determine the ideal size and configuration of HRES comprised of PV, wind turbines, diesel generators, and batteries. The primary objectives of their developed optimisation model were based on technical, social and economic perspectives. It has been established that an HRES consisting of 78.44 kW PV systems, 95 kW wind turbines, and a 2 kW battery is the ideal

* Corresponding author.
E-mail address: Manosh.Paul@glasgow.ac.uk (M.C. Paul).

https://doi.org/10.1016/j.enconman.2023.117444
Received 13 March 2023; Received in revised form 19 June 2023; Accepted 22 July 2023

Nomenclature

Abbreviations

HRES	Hybrid renewable energy system
PHES	Pumped hydropower energy storage
ESS	Energy storage system
REF	Renewable energy fraction (%)
LORE	Loss of renewable energy (%)

Symbols

A_{res}	Surface area of the reservoir (m^2)
A_{bl}	Wind turbine swept area (m^2)
a	Diode ideality factor
C_p	Power coefficient for wind turbine
C_{pipe}	Total cost of pipe ($)
$C_{E,loss}$	Total cost of energy loss ($)
d	Pipe diameter (m)
ET	Reference evapotranspiration (mm/hour)
E_{grid}	Energy supplied by the natural grid (MWh)
E_{lost}	loss of renewable energy (MWh)
$E_{lost,H}$	Total energy lost caused by head loss (MWh)
E_{demand}	Energy demand (MWh)
E_{solar}	Solar energy (MWh)
E_{wind}	Wind energy (MWh)
E_{pump}	Electricity used to pump water (MWh)
$E_{turbine}$	Electricity produced by PHES (MWh)
E_{RES}	Energy produced wind + PV + PHES (MWh)
E_{excess}	Surplus renewable energy (MWh)
$E_{shortage}$	Energy demand needed to be met (MWh)
E_{cost}	Cost of electricity ($/kWh)
Elv	Height of the wind turbine hub (m)
$Elv1$	Height as the reference (m)
e^0	Saturation vapour pressure (kPa)
e_a	Actual vapour pressure (kPa)
f	Friction factor inside pipe
G_t	Irradiation at module surface(W/m^2)
g	Gravity acceleration (m/s^2)
H_{tu}	Head loss in generating mode (m)
H_{pu}	Head loss in pumping mode (m)
H_{st}	Static head (m)
H_{loss}	Total head loss (m)
H_{ratio}	Ratio of head loss
H_v	Distance among upper & lower reservoir (m)
H_{lup}	Water level in the upper reservoir (m)
H_{up}	Upper reservoir height (m)
I	PV output current (A)
I_{pv}	Photocurrent (A)
I_0	Diode saturation current (A)
I_{sc}	Short circuit current (A)
K_I	Temperature coefficient (A/°C)
K_v	Temperature coefficient (V/°C)
k	Boltzmann constant ($1.38064852 \times 10^{-23}$J/K)
K_{pipe}	Pipe resistance coefficient
$K_{fittings}$	Fitting resistance coefficient
L	Pipe length (m)
N_{pv}	Number of PV modules
N_{wind}	Number of wind turbines
$N_{P/T}$	Number of reversible pump/turbines
N_s	Number of connected cells
$N_{turbines}$	Number of PHES turbines
N_{pump}	Number of PHES pumps
P_{pv}	PV module power (W)
PR	Performance ratio of PV (0.7)
$P_{max,cal}$	Maximum power of PV module (W)
P_{wind}	Wind power (MW)
P_P	Power needed to pump water (MW)
P_T	Power generated by turbine (MW)
q	Electron charge ($1.6021766208 \times 10^{-19}$ °C)
Q_P	Flow rate in pumping mode (m^3/s)
Q_T	Flow rate in generating mode (m^3/s)
R_p	Parallel shunt resistance (Ω)
Re	Reynolds number
S_v	Saturation slope vapour pressure (kPa/°C)
S_{he}	Soil heat flux density (MJ/m^2/hour)
T	Actual cell temperature (°C)
T_a	Ambient temperature (°C)
t	Interval time (hour)
U_L	Loss coefficient
u_z	Wind speed at reservoir (m/s)
V_t	Thermal voltage of the module (V)
V_{oc}	Open circuit voltage (V)
V_{pre}	Volume in previous interval time (m^3)
v	Average wind speed at the hub (m/s)
v_1	Wind speed -elevation of 10 m (m/s)
V_e	Volume of evaporated water (m^3)
$V_{reservior}$	Availability of upper reservoir (m^3)
V_f	Flow velocity (m/s)
$V_{f.max}$	Maximum flow velocity (m/s)

Greek Symbols

η_{wg}	Generator/rotor power efficiency of wind turbine
η_c	Solar module efficiency (%)
η_{tu}	Turbine efficiency (%)
η_{pu}	Pump efficiency (%)
α	Wind profile exponent equals to 1/7
ρ_{water}	Density of water (kg/m^3)
$\alpha\tau$	Effective transmission-absorptance
ε	Absolute roughness
ρ_{air}	Air density (kg/m^3)
γ	Psychrometric constant (kPa/°C)

Subscripts

T	The turbine
P	The pump
C, N	Considered, Neglected scenario

configuration in terms of the proposed model's objectives. In addition, using identical HRES components, a comparative analysis of two optimisation techniques—conventional and swarm intelligence based—to design each component was carried out in [5]. The final outcomes of both approaches were nearly equivalent. Furthermore, Nasser et al. [6] have conducted a techno-economic optimisation model utilising System Advisory Model (SAM) software to design HRES comprised of PV, wind turbines and PHES. It was then revealed that the implementation of such a system is effective in terms of total cost and overall reliability. The fluctuation of RES and electricity demand are crucial aspects for sizing HRES; therefore, combining two methodologies—mixed integer modelling and artificial neural networks—has been proposed [7] to address this issue. This study applied a hybrid system comprised of PV, wind and PHES, and it was observed that this strategy might reduce the impact of RES variability when connected to the natural grid. Using two distinct types of ESS, such as PHES and batteries, combined with PV and

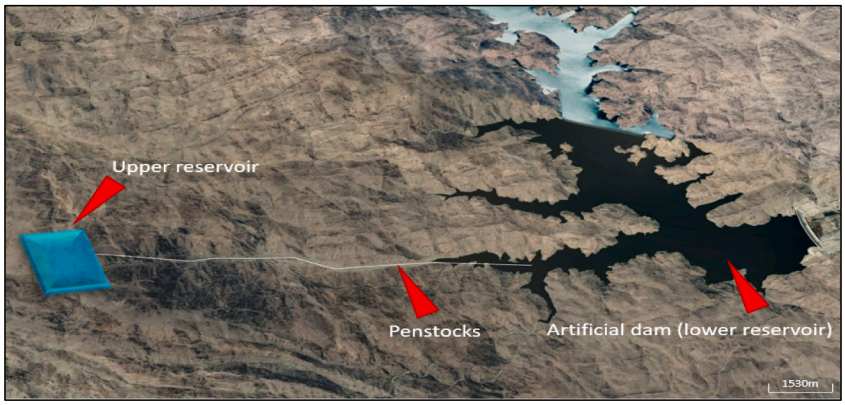

(a)

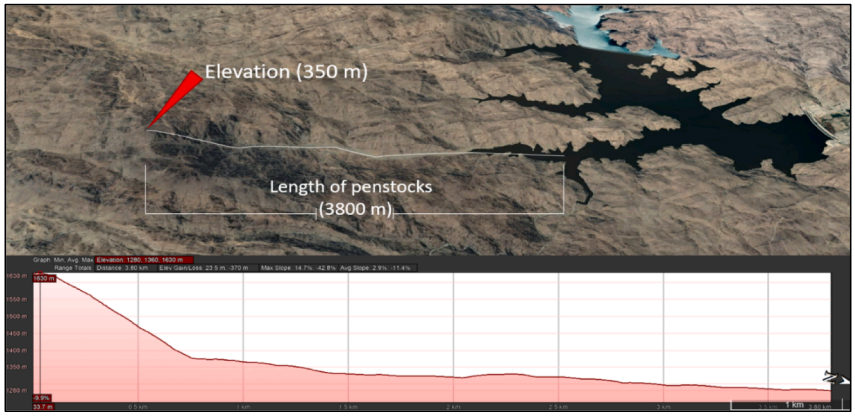

(b)

Fig. 1. (a) Proposed site of PHES, (b) Elevation between lower and upper reservoirs [Note: *These figures are produced using the Google Earth program].*

wind turbines, has been investigated previously in two studies [8,9]. According to these studies, the proposed HRES is a viable option from both technical and economic viewpoints. Considering the similar RES and ESS applied in the aforementioned studies, further research with various purposes has been undertaken. For example, Tao Ma and Muhammad Javed [10] conducted a techno-economic optimisation model, with the main focus on increasing the saturation level of RES; Portero et al. [11] considered seawater exploitation for sizing PHES; Bahadur Pali and Shelly Vadhera [12] proposed a novel technique aiming to maintain power generation with a constant voltage; and Ming et al. [13] developed a robust optimisation model for energy management improvement.

However, sizing the capacity of RES or ESS components requires an accurate numerical model to simulate and study the actual performance of HRES. Some ESS includes subcomponents that make the entire simulation of the system more complicated, such as the PHES, which consists mostly of pumps, turbines, two reservoirs, and a pipe. Moreover, when PHES is connected to multiple sources of RES, the accuracy of the PHES model's simulation might affect the performance of the entire HRES. A study was carried out [2] that considered some critical parameters (i.e., hydraulic losses of the turbine) to increase the accuracy of the modelling of the PHES system. The developed PHES model was based on experimental results and was compared with various other models. Furthermore, the model was tested and analysed for a period of 10 days, eventually resulting in an increase in the simulation accuracy of the PHES system. The critical parameters in the mathematical model, as well as any factor that has a noticeable impact on system performance, should be carefully addressed. As a result, not taking into account these critical parameters or factors when designing such a system may result in errors in the final stage of planning, which are the primary reasons for the fluctuations in the accuracy of an HRES model's outcomes. However, the upper reservoir's water volume during charging and discharging is significantly influenced by the total head loss (H_{loss}) and rate of evaporation, and thus considering these factors, especially with a closed-loop PHES (where there is no river or very little flow of natural water sources) become more essential in a simulation model of PHES. These elements are becoming increasingly essential for a location that has a very hot climate during summer and has no rivers or continuous inflows of water, such as Saudi Arabia. This country is located in the Middle East and is one of the largest oil exporters worldwide. It has an area of 2.15 million km^2, a population of more than 33 million people and is one of the largest Middle Eastern countries [14]. Because of the rapid growth in the population, annual electricity demand has increased by 8–10% [15]. In addition, because of the significant reliance on conventional power plants to meet the demand with more than seventeen power plants, renewable energy installation of more than 40 GW by 2030 is targeted [16]. As such, this target corresponds to an enormous capacity, which considerably requires appropriate energy storage to avoid the loss of renewable energy. There is a clear possibility of utilising artificial dams in the southern region and building an upper reservoir on top of the surrounding mountains with high elevation [17,18]. These studies looked into the possibility of installing PHES in some locations in Saudi Arabia, and it was suggested that seasonal dams be used for closed-loop storage, with upper reservoirs built in the surrounding mountains. The southern region of Saudi Arabia, specifically Bisha city, has the largest artificial reservoir, which is considered to be a suitable site to install a closed-loop PHES, as illustrated in Fig. 1. The total storage capacity of an artificial reservoir is 325 million cubic metres with a dam wall height of 103 m [17].. Based on the design performed in this study, depending on the topographical information as shown in Fig. 1,(a-b), there is an

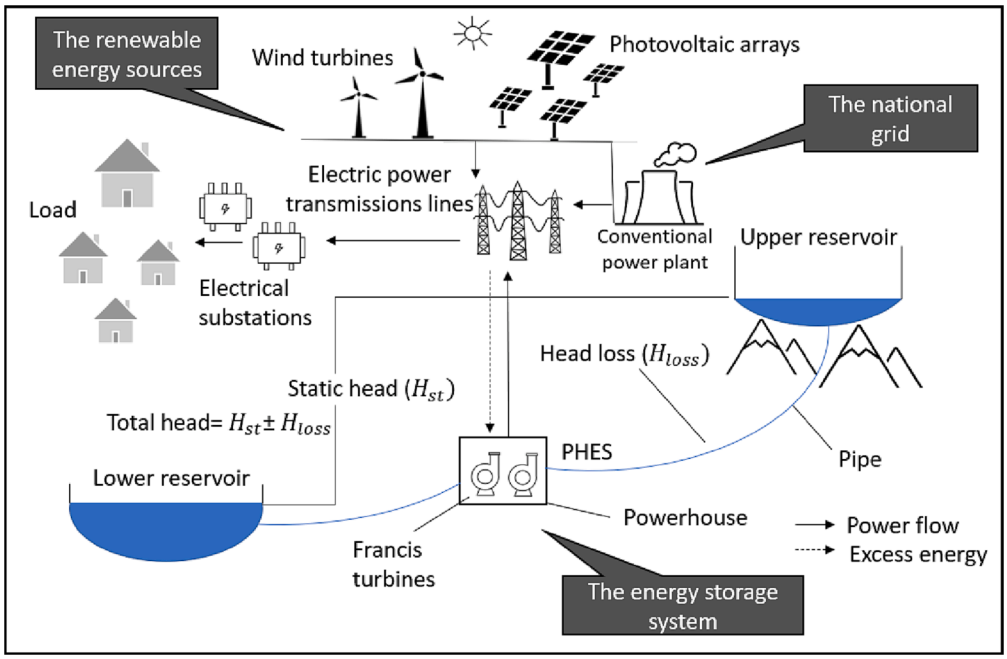

Fig. 2. Systematic diagram of the proposed HRES.

excellent potential to build an upper reservoir on the top of mountains with an elevation of up to 350 m. In addition, the ideal elevation between two reservoirs is examined. Since the PHES is a large-scale power system, a significant concern is whether a suitable energy storage capacity will be implemented to avoid losing a substantial amount of renewable energy [19]. Because of that, a technical feasibility study that investigates the behaviour of the proposed system, while taking into account total H_{loss} and rate of evaporation, has been strongly recommended.

2. Research gap and contribution to the knowledge

To the best of the authors' knowledge, the performance of an HRES with a large-scale PHES when connected to a national grid has not been extensively investigated. Therefore, there is a relative lack of information in the published studies in this context that focus exclusively on improving the accuracy of a PHES simulation process. Thus, a significant knowledge gap can be observed, which has been filled by the research presented in the current paper. However, based on the literature review, the H_{loss} and evaporation rate assigned in the PHES model were neglected or considered constant parameters that were assumed in the simulation process because their impact on the overall system performance was reported to be either slight or for a study simplification. Furthermore, determining H_{loss} as a variable in the mathematical model of PHES requires comprehensive techno-economic analysis to accurately size the PHES pipe where H_{loss} mainly occurs. Additionally, whether in a pumping or generating mode, the real H_{loss} changes depending on the amount of available power to pump water and the amount of flow rate required to produce a specific amount of energy. Some studies considered the H_{loss} factor by assuming the pipe diameter or determining it based on empirical analysis. However, disregarding/miscalculating H_{loss} and the evaporation rate may cause a decrease in the accuracy of the overall PHES simulation performance, resulting in an underestimation of the proper size of each HRES component. A novel HRES–PV and wind-connected PHES is presented, and the present study aims to increase the simulation accuracy of HRES by considering the two main study indicators: renewable energy fraction (*REF*) and loss of renewable energy (*LORE*), which are the essential technical indicators employed for designing the HRES. To successfully accomplish the goal of the present study, some objectives have been proposed, as follows:

- Determine the effective evaporation rate of large-scale closed-loop storage based on hourly meteorological data and conduct critical assessments for the summer and winter seasons.
- Propose a novel technique and framework allowing for and facilitating the HRES project designers at the initial technical analysis to select the optimal and suitable size of pipe used in PHES based on a thorough techno-economic analysis and determine the precise H_{loss} for pumping and generating modes.
- Conduct a comprehensive technical analysis of the impact of large-scale PHES model accuracy with considering/neglecting head loss parameters on the physical behaviour of an integrated RES and accuracy of simulation performance by considering variations in the main influential variables (e.g., the capacity of RES and PHES). This analysis is performed for long- and short-term assessments.

3. Methods

This section discusses the proposed HRES and its operating strategy while also describing the problem. Additionally, a full techno-economic evaluation of selecting a suitable pipe design, assessment procedures and variations in the system design variables are presented.

3.1. The proposed hybrid renewable energy system

The HRES presented in Fig. 2 comprises PV, wind turbines and PHES as the energy storage system. The PHES is mostly composed of two reservoirs (upper and lower), pump, turbine, and pipe. Then, the HRES is considered a grid-on utility-scale system which may cover most of the electricity demand at a specific location, as explained in Section 1. The hourly electricity demand (E_{demand}) is supposed to be met by the amount of available renewable energy ($E_{pv+wind}$) or energy produced by PHES turbine ($E_{turbine}$); however, if the demand is not fulfilled, it is met by the national grid (E_{grid}). On the other hand, the excess renewable energy (E_{excess}) is exploited to pump water from a lower reservoir to an upper reservoir. If the water level in the upper reservoir reaches its maximum capacity, the remaining energy will be accounted for as a loss of renewable energy (E_{lost}). The PHES is designed as a closed-loop system,

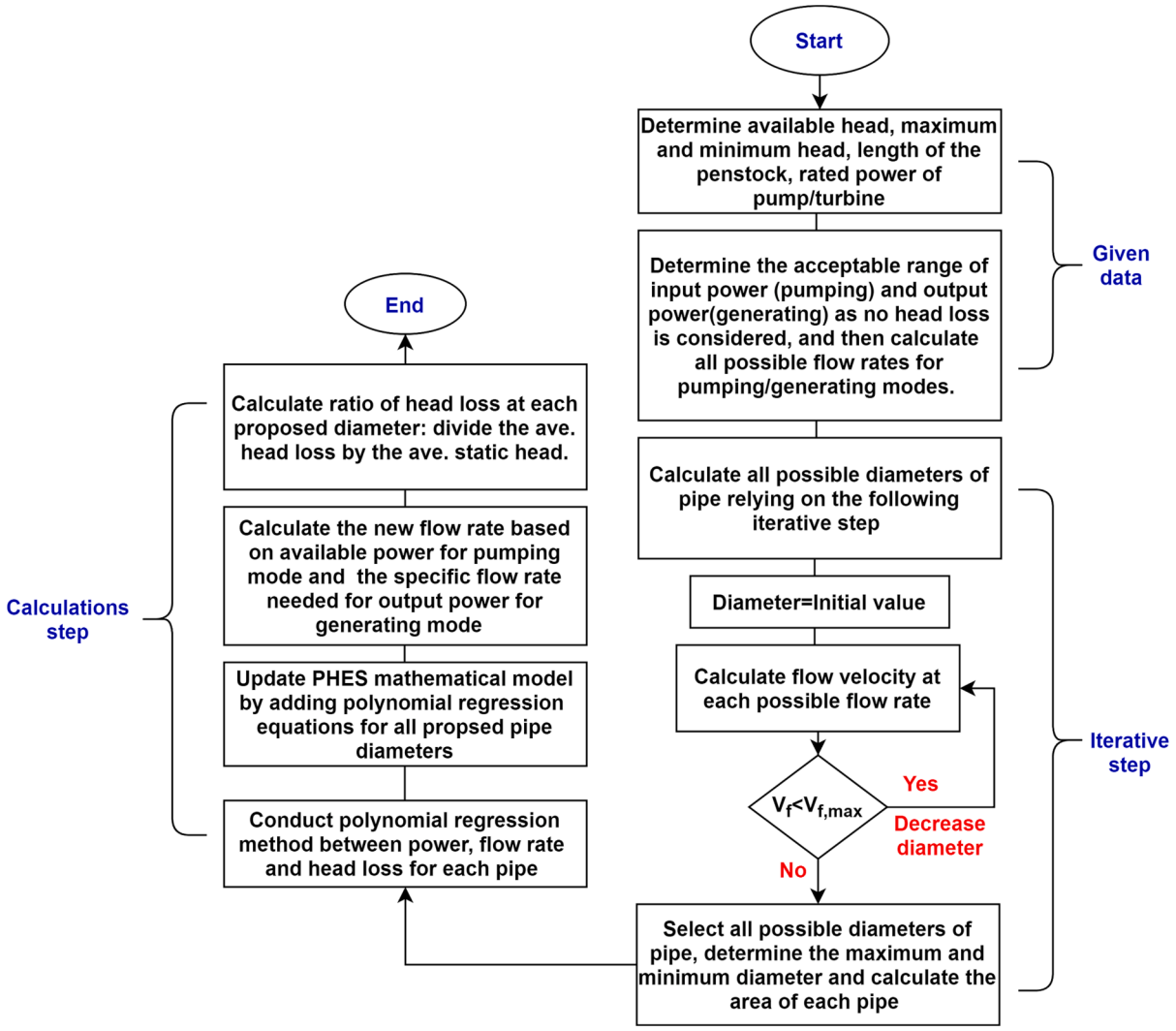

Fig. 3. The proposed procedure for pipe design technical assessment.

which means there is no water waste since this case study has no continuous water flow such as a river, but instead uses an existing large dam which has a massive amount of water [18]. Each component connected to the HRES is mathematically modelled to build a simulation tool in Python for the entire system performance, and the hourly operation of the HRES is validated based on the energy balance approach on the basis of one hour for 8760 h (further details are in Appendix A.). The way the HRES is interfaced is based on the proposed energy dispatch strategy, as explained in Section 2.3.

3.2. Problem formulation

The HRES is intended to play an essential role in reducing the reliance on conventional power plants, but it requires more attention to accurately size each component by considering the essential factors in the simulation process. Then, for the closed-loop system of PHES (with no continuous water source), as proposed in the present study, which is located in dry or hot climates, the evaporation rate becomes an essential parameter; thus, it has been predicted for the entire year on an hourly basis. Another essential factor is H_{loss} occurring inside the pipe connected between two reservoirs in PHES.The H_{loss} is mainly classified into minor (because of valves, fitting, etc.) and major losses (because of friction in the pipe) and is primarily influenced by certain essential factors: the amount of flow rate inside the pipe, flow velocity and pipe design. To determine the accurate H_{loss} in the PHES simulation process, the pipe is the most significant component. Therefore, the design of the pipe (length and diameter) should be properly carried out. In the present study, the length of the pipe is assumed constant because the elevation between the two reservoirs remains fixed, based on the initial geographical evaluation, here with a value of 3800 m, as shown in Fig. 1. As a result, only the pipe diameter is assumed to be variable when designing an appropriate pipe. To identify the most suitable pipe diameter, a comprehensive techno-economic assessment is essential. After conducting this analysis, the optimum pipe diameter is selected based on the designer's preferences. The present study proposes that the optimum pipe diameter should meet the two technical constraints outlined in Section 2.2.1 and be economically viable according to the approach stated in Section 2.2.2. In addition, because of the requirement for study simplicity and emphasis on a technical rather than economic analysis of H_{loss}, the current study has a limitation. H_{loss} is solely affected by the specific pipe design, any economic analysis associated with the specific HRES or PHES components (except pipe) is disregarded, and only an assessment of large-scale HRES and PHES is considered.

3.2.1. Technical analysis

Regarding the boundaries of the pipe design, an appropriate pipe diameter to be used in the PHES should be selected based on the two main proposed technical conditions. These conditions are that the fluid velocity (V_f) inside the pipe should be lower than 10 m/s ([20,21]), and the preferred head loss ratio (H_{ratio}) is less than 15% ([22,23]) which is

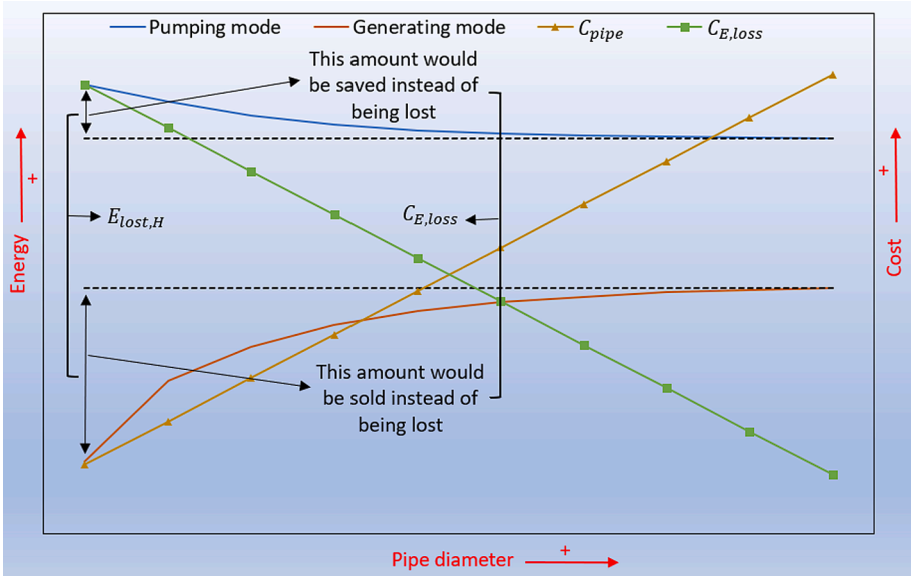

Fig. 4. A typical relationship between energy, pipe diameter and cost.

calculated using a fraction of the H_{loss} for the specific pipe diameter divided by the average static head.The reason behind setting the maximum water velocity ($V_{f,max}$) at 10 m/s is that increasing the V_f above this limit might cause significant consequences, such as cavitation [20]. To calculate the amount of flow rate for pumping (Q_P)/generating mode (Q_T) and V_f inside the penstock, first, the diameter of the penstock needs to be known (the mathematical model for that is explained in Appendix A.**3)**. Then, an acceptable range of the pipe diameter is calculated based on an iterative method between all the suggested pipe diameters, here beginning with an initial value that is a typical large diameter; this value decreases slightly until the proposed $V_{f,max}$ is reached. Also, Q_P and Q_T are calculated based on the design of the two reservoirs of the PHES, the elevation-length between them, and the capacity of the pump/turbine based on the specific location and E_{demand}. The minimum and maximum amount of Q_P and Q_T are then determined based on the maximum and minimum power for the pumping mode (P_P)/generating mode (P_T) for all the possible states of the charging /discharging process, respectively. After all the potential pipe diameters become known with the first condition satisfied, the actual H_{loss} for the pumping mode (H_{pu}) and for the generating mode (H_{tu}) is determined, and it varies with the specific pipe diameter based on the E_{excess} for the pumping mode and the $E_{shortage}$ for the generating mode. Therefore, a correlation between P_P, H_{pu} and H_{tu}, Q_T for each suggested pipe diameter is developed, and a polynomial regression method with high R-squared results is used. Subsequently, H_{ratio} for each pipe diameter is determined to investigate which pipe diameter satisfies the second technical condition. Importantly, considering H_{pu} may reduce the total of E_{lost} because of an increased usage of electricity and in contrast for the generating mode, the $E_{turbine}$ may decrease. This however depends on the HRES design in terms of the capacity of each component connected to the system. Then, all these data are normalised and combined in order to trade-off between all the variables of H_{pu}, H_{tu} and E_{pump},$E_{turbine}$ for the long-term assessment 8760 h. This relies on designer desires, and in this study the intersection point between all these variables is considered as a compromised design. Eventually, the entire proposed technique is concisely presented in Fig. 3.

3.2.2. Economic analysis

It is known that the H_{loss} parameter is directly influenced by the pipe design ([24,25]). Therefore, the essential variables in selecting the most economical pipe diameter are the total annualised cost of the pipe (C_{pipe}) and the value of energy loss ($C_{E,loss}$), which are triggered by a specific amount of H_{loss}. Basically, when the pipe diameter increases, H_{loss} decreases, while the C_{pipe} and the profit of PHES increase simultaneously. Thus, an economic optimisation between these two variables was conducted. As a result, both C_{pipe} and $C_{E,loss}$ were calculated for a particular lifetime of the penstock ([26]). This study used the electricity cost (E_{cost}) per kWh for the pumping and generating modes. This specific cost was multiplied by the total energy loss occurred by considering the head loss ($E_{lost,H}$) to calculate the total $C_{E,loss}$. Fig. 4 shows a typical relationship between all the variables related to H_{loss} (energy consumed(pump)/produced(turbine), pipe diameter and cost). It also reveals that E_{pump} (blue line) decreases and $E_{turbine}$ (brown line) increases by raising the pipe's diameter (green line). Fig. 4 also shows that by increasing the pipe's diameter, more energy would be gained in the generating mode and less energy would be consumed in the pumping mode. Therefore, $C_{E,loss}$ is calculated based on the sum values of $E_{lost,H}$ multiplied by E_{cost} in the pumping and generating modes. Next, the optimisation between C_{pipe} and $C_{E,loss}$ is conducted, and the optimal pipe diameter based on the techno-economic analysis is designated.

3.3. Assessment procedure

Following the selection of an appropriate pipe diameter (based on the techno-economic analysis) and the provision of the polynomial regression equations to predict H_{pu} and H_{tu}, the performance of HRES has been comprehensively evaluated. Moreover, the *REF* and *LORE* have been selected as the study performance indicators as they are considered the most common technical indicators needed to design the HRES, as expressed in Eqs. (1)-(2). The simulation tool of the entire HRES is built based on the proposed energy dispatch strategy on the basis of one hour, as illustrated by the green font colour in Fig. 5. The comprehensive assessment of how the H_{loss} parameter is essential has been conducted with two different scenarios in terms of considering (C) or neglecting (N) this parameter. This assessment is accomplished by performing a comparative analysis within these two scenarios for the short-term (several days) and long-term (8760 h) assessments with given data for all the variables. So, in this study, the design of HRES includes four different variables: the number of PV panels (N_{pv}), wind turbines (N_{wind}), pumps /turbines $N_{P/T}$ and the capacity of upper reservoir of PHES (V_{res}). Therefore, an iterative method between the diverse design configurations with predefined variables values is proposed to evaluate the

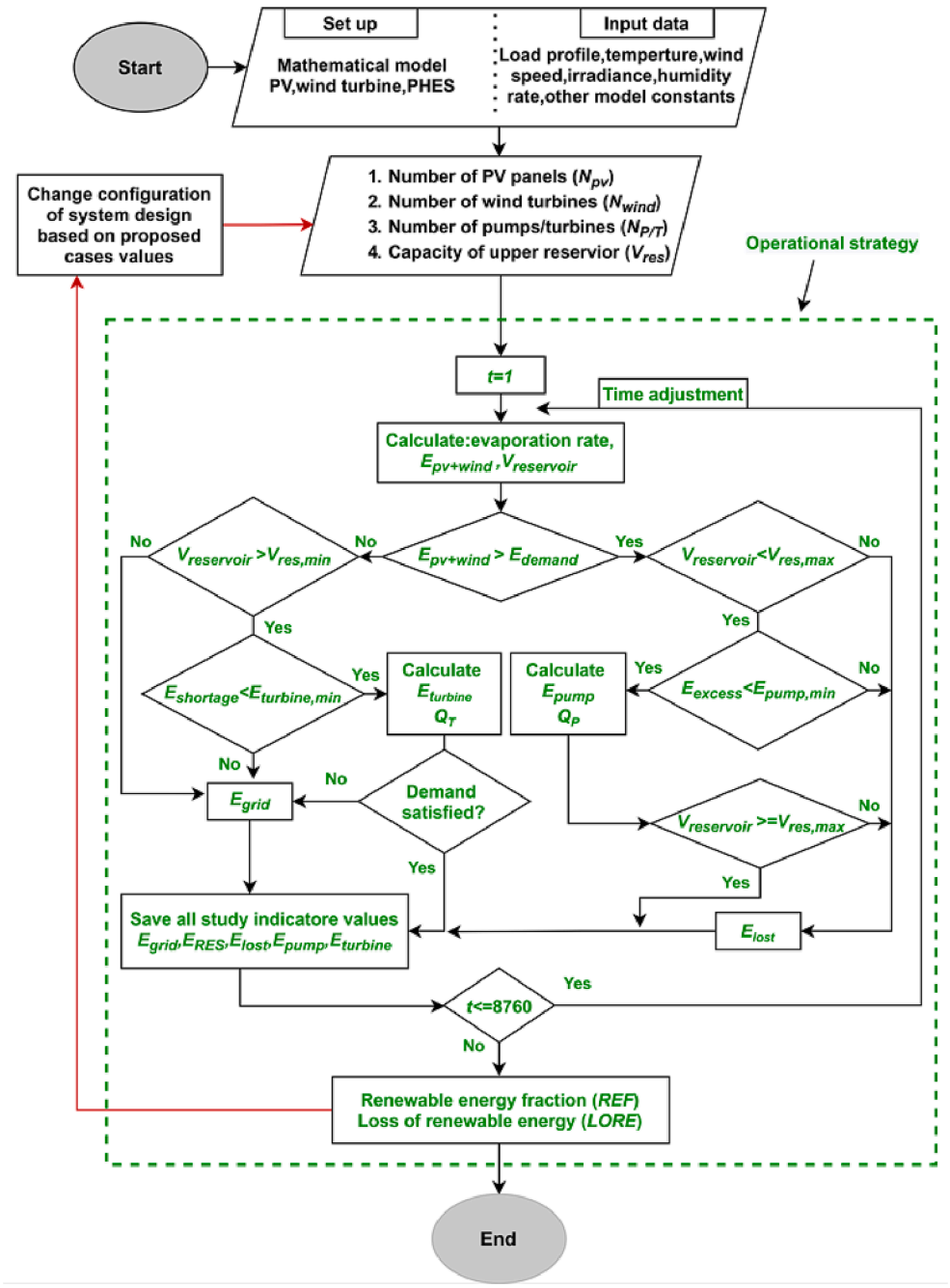

Fig. 5. Flow chart of operation strategy of HRES.

relationship between sizing the HRES components, applying the proposed technique, considering H_{loss} in the simulation process, and investigating the most influential variables that impact the HRES performance. The iterative method between all the variables and proposed cases is summarised and demonstrated in Section 2.4.

$$REF(\%) = \sum_{t=1}^{t_{end}} \frac{E_{demand}(t) - E_{grid}(t)}{E_{demand}(t)} \times 100 \quad (1)$$

$$LORE(\%) = \sum_{t=1}^{t_{end}} \frac{E_{lost}(t)}{E_{solar}(t) + E_{wind}(t)} \times 100 \quad (2)$$

$$E_{lost}(MWh) = \sum_{t=1}^{t_{end}} E_{solar}(t) + E_{wind}(t) - E_{pump}(t) - E_{demand}(t) + E_{grid}(t) + E_{turbine}(t) \quad (3)$$

$$E_{RES}(MWh) = \sum_{t=1}^{t_{end}} E_{demand}(t) - E_{grid}(t) \quad (4)$$

3.4. Variations in system design configurations

A total of thirty-six different configurations of HRES design have been investigated considering the ten various installed solar energy capacities, ten different installed wind energy capacities, ten different pump/turbine capacities, and ten different upper reservoir capacities, as provided in Table 1. The reason behind dividing each variable into ten

Table 1
Variation in installed renewable energy capacity.

All cases	N_{pv} ** Panels (M)	E_{pv} * (MW)	N_{wind} Wind turbines	E_{wind} * (MW)	$E_{pv+wind}$ (MW)	$N_{P/T}$ turbines	V_{res} ** (m^3)
$Case_1$	0.5	100	100	200	300	1	2 M
$Case_2$	1	200	150	300	500	2	3 M
$Case_3$	1.5	300	200	400	700	3	4 M
$Case_4$	2	400	250	500	900	4	5 M
$Case_5$	2.5	500	300	600	1100	5	6 M
$Case_6$	3	600	350	700	1300	6	7 M
$Case_7$	3.5	700	400	800	1500	7	8 M
$Case_8$	4	800	450	900	1700	8	9 M
$Case_9$	4.5	900	500	1000	1900	9	10 M
$Case_{10}$	5	1000	550	1100	2100	10	11 M

* These values are ideal before considering the total efficiency and other effective parameters (i.e., Meteorological data).
** M refers to a Million.

prominent cases and the size of each component's assumption is based on the average actual electricity demand data for the adopted location and its topography information. With regard to wind and solar energy, the maximum and minimum electricity demand over the entire year is determined, and thus all the case values are investigated. The minimum capacity of wind and solar energy that has been set up is 200 and 100 MW, and they increase in steps of 100 MW, respectively, until they reach $Case_{10}$ with values of 1.1 GW for the wind and 1 GW for solar, respectively. On the other hand, the PHES capacity is estimated chiefly based on the volume of the upper and lower reservoir, the capacity of the pump/turbine, and the static height between the two reservoirs. The variation in the upper reservoir capacity, which is arbitrarily considered to be 2–11 Mm^3 in the step of 1 Mm^3 and the capacity of pump/turbine (1–10 pumps/turbines increase in the step of one at each case) with a rated power of 75 MW, respectively, has been determined relying on the performed design. As shown in Table 1, the maximum and minimum values of each variable correspond to $Case_1$ and $Case_{10}$, respectively. The way to show the total simulation results for proposed configurations is to evaluate one variable for each case while the other variables were constant with the maximum number as presented in $Case_{10}$. For example, when the variable (N_{pv}) is being evaluated gradually from $Case_1$ (100 MW) to $Case_9$ (900 MW), the other variables (N_{wind}, $N_{P/T}$, V_{res}) simultaneously remain constant with the values of maximum in $Case_{10}$ and so on.

4. Results and discussion

With regard to the meteorological data for the adopted location (Saudi Arabia), the solar radiation, wind speed, and temperature for one whole year on the basis of one hour for the specific city (Bisha) have been collected from the National Solar Radiation Database (NSRDB) [27]. In addition, the actual electricity demand data of Bisha has been collected from the Saudi electricity company for the entire year on an hourly basis [28]. All of these data are presented as monthly-average hourly for the entire year in Fig. 6. From the same figure, it can be seen that the temperature increases during the summer season, reaching 38 °C and this may influence the PV system performance as well as the water stored in reservoir in terms of the evaporation rate. The most remarkable solar radiance appears to be in May, unlike December where the lowest rate occurs. In addition, the wind speed seems to be high during summer and stays at almost the same range for the other seasons. The electricity demand almost has similar trends from January to April, and then it starts increasing until September when it clearly goes down to its original starting point. The total electricity consumption of Bisha for 8760 h is approximately 2.497 TWh.

4.1. Evaporation rate

The evaporation rate has been adopted in this study to assess the amount of evaporated water from the upper reservoir for 8760 h based on Eq. (A.18); the evaporation rate of the lower reservoir (adopted dam) has been neglected because of the fluctuation of inflow water which is caused by an unknown precipitation amount adding to a massive area of the adopted dam. Fig. 7-(a) shows evaporated water for four days in both the winter and summer periods. It is evident that the increased rate during daylight is because the summer season experiences more high temperatures, reaching up to 1.2 mm, compared to 0.64 mm in the winter season. The total monthly evaporated water is shown in Fig. 7-(b), and it shows that the highest point, of up to 338 mm, occurs in July. Conversely, the lowest point is in January, with 169 mm. The summation of all months, which is considered annually evaporated water, is 3042 mm. This amount is remarkable as the PHES is a closed system, and there is no continuous inflow of water. Therefore, when the simulation is performed for the long term (8760 h) and neglecting this amount of actual evaporated water, the accuracy of the entire system performance in terms of energy management might be reduced. In addition, when installing a lower reservoir instead of using the adopted dam, this particular point becomes an essential parameter for designing the HRES.

4.2. The pipe design assessment

Based on the proposed technique illustrated in Section 2.2, the precise, iterative step of discovering all the possible pipe diameters, the V_f of each proposed pipe is determined. As the iterative step regarding V_f in the proposed technique is set decreasing by 0.2 m at each iteration, the maximum and minimum proposed diameter of pipes are found to be 3.4 m and 1.6 m, respectively, with respect to the design boundaries. Fig. 8-(a,b) shows the amount of V_f inside each proposed pipe for the pumping

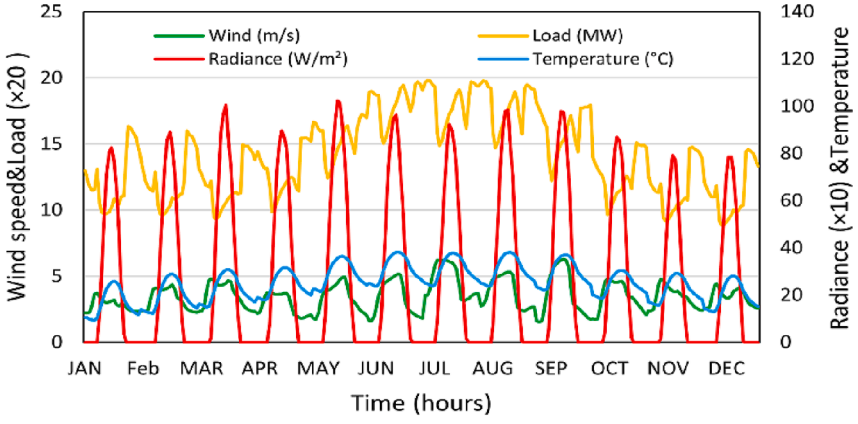

Fig. 6. Meteorological data and electricity demand of the adopted site.

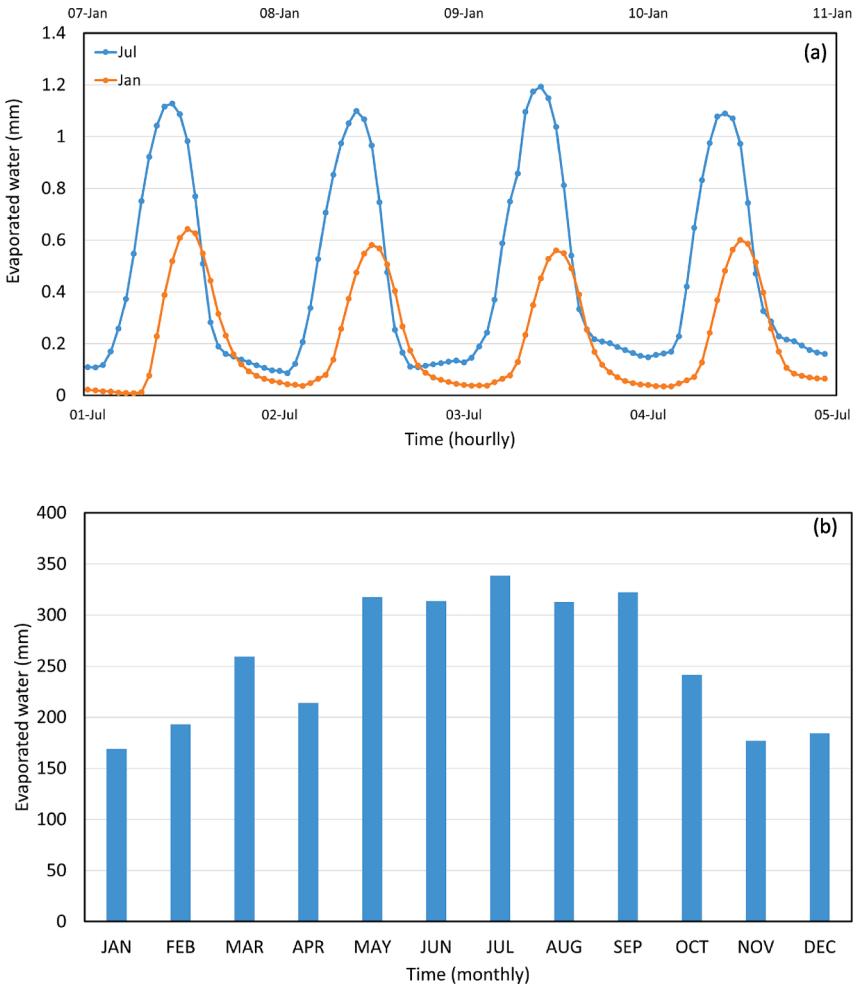

Fig. 7. Amount of evaporated water (a) four days in summer (July) and winter (January) seasons, (b) over one year.

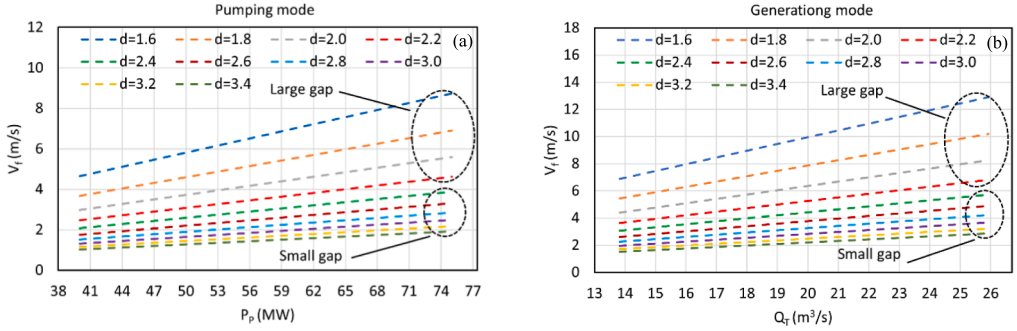

Fig. 8. The water velocity inside penstock for each possible pipe diameter: (a) pumping mode (b) generating mode.

/generating modes and considering all the possible working states (charging/discharging). Therefore, it should be highlighted that the *x*-axis in the pumping mode in Fig. 8-(a) is different from the generating mode in Fig. 8-(b) and because of that the Q_P is calculated based on E_{excess}, unlike in the generating mode in which the Q_T is calculated based on $E_{shortage}$. Then, for the pumping mode, as shown in Fig. 8-(a), it is evident that the V_f for each proposed pipe is under 10 m/s respectively, with the highest value of approximately 8 m/s occurring with a diameter of 1.6 m. In contrast, the highest V_f of 12 m/s occurs with a pipe diameter of 1.6 m in the generating mode, as shown in Fig. 8-(b). This exceeds the $V_{f,max}$ (10 m/s) at the final iteration, and it is not even considered as a proper choice, but it can be seen how a small diameter causes a very high amount of V_f. Significantly, from the pumping/generation modes results, it is shown that when the pipe diameter decreases, the gap between the rate of V_f of each pipe is relatively small until reaching a diameter of 2.2 m where the gap starts rising until last diameter, as illustrated in Fig. 8-(a,b) by a dashed circle. In addition, it is clear that the gap between the four different pipe diameters of 1.6, 1.8, 2, and 2.2 m is almost equal to the difference between the six larger pipe diameters 2.4, 2.6, 2.8, 3.0, 3.2, and 3.4 m, respectively.

Following the range of the pipe diameter, the amount of H_{loss} for each pipe is determined. As it can be seen in Fig. 9 that each pipe diameter

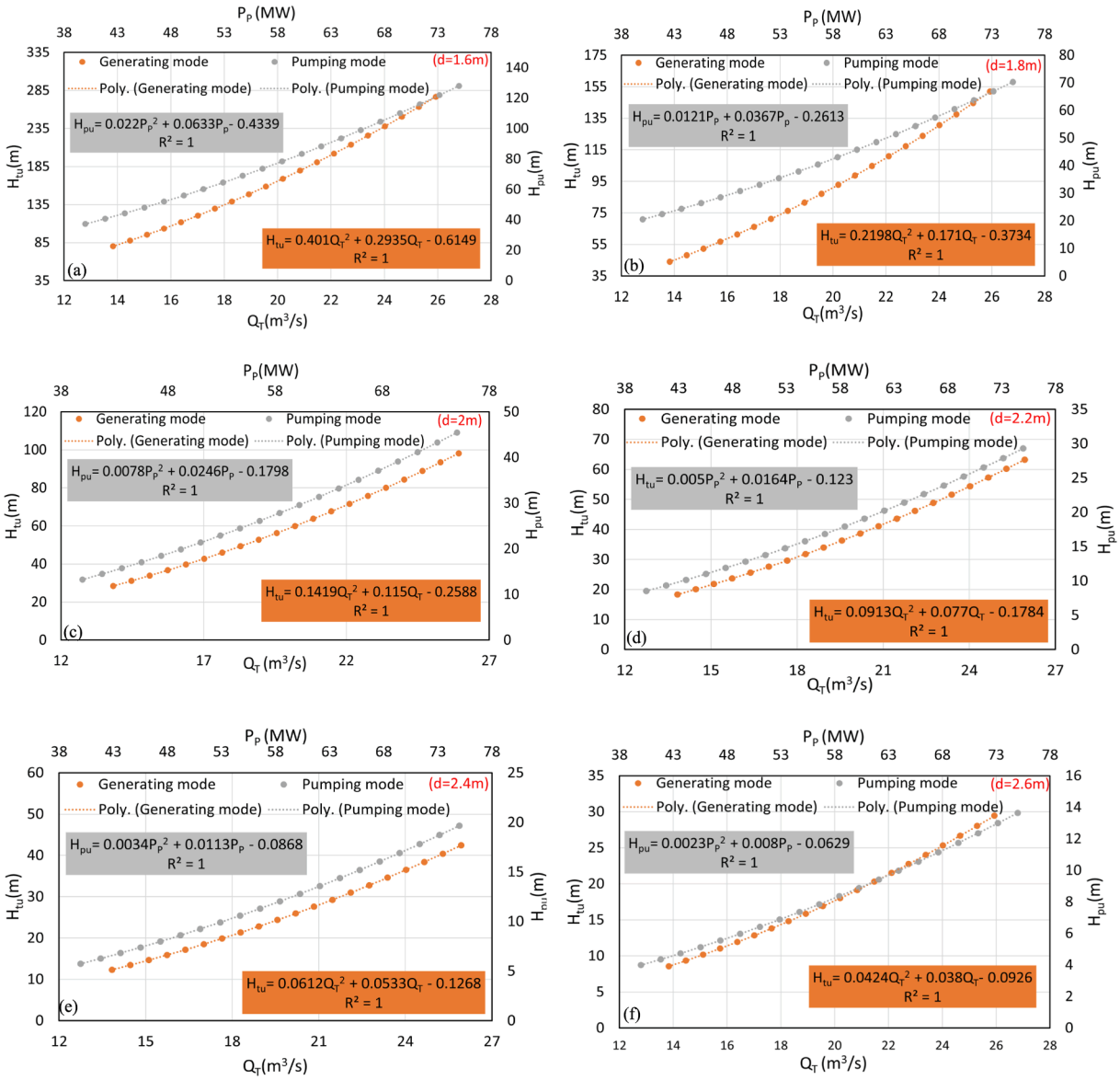

Fig. 9. The polynomial regression results for pumping and generation modes for all the possible pipe diameters.

includes two regression equations based on the value of H_{pu} associated with P_P (second x-axis) and H_{tu} correlated with Q_T (main x-axis). The reason behind conducting the regression approach for each proposed pipe is that when the total of E_{pump} and $E_{turbine}$ are calculated using the simulation tool, there should be equations to predict H_{loss} based on the available amount of E_{excess} and $E_{shortage}$. Fig. 9-(a, j) show all the possible values of H_{pu} and H_{tu} for each pipe with the corresponding regression equations for the pumping/generation mode. From Fig. 9-(a), it can be seen that the maximum H_{pu} occurs with a pipe diameter of 1.6 m with a value of 286 m in the generating mode. In contrast, the lowest H_{tu} occurs with a value of 9 m respectively with a pipe diameter of 3.4 m, as shown in Fig. 9-(j).

4.2.1. Technical evaluations

The most critical step in the proposed technique is how to select the most appropriate pipe diameter satisfying the proposed technique conditions and then inserting the regression equations of H_{loss} for pumping and generating into the PHES mathematical model. To calculate the new total of E_{pump} and $E_{turbine}$ for 8760 h, all the input data in the simulation tool should be known. N_{pv} and N_{wind} are specified as assumed in $Case_{10}$ (Table 1) to increase the usage rate of PHES. With regard to the PHES capacity which relies on the two different variables (V_{res} and $N_{P/T}$), the maximum and minimum capacity of these variables, as proposed in $Case_1$ and $Case_{10}$, have been assessed. As E_{pump} is determined based on E_{excess}, it is clear from Fig. 10-(a) that when the pipe diameter increases, E_{pump} and H_{ratio}(P) decrease while the E_{lost} slightly increases. On the other hand, $E_{turbine}$ increases while the pipe diameter and H_{ratio}(T) decreases because H_{loss} in the larger pipe diameter is lower than that in the smaller diameter. Therefore, the correlation data between the two variables E_{lost} and E_{pump}, and the two other variables, H_{ratio}(T) and $E_{turbine}$ should be analysed. So, the data normalisation for all the variables together for the pumping /generating modes helps to see the correlation between them. (See Table 2)

4.2.2. Economic evaluations

With all the proposed technical conditions satisfied and all the appropriate pipe diameters determined, an economic analysis was conducted based on the method explained in Section 2.2.2. To avoid any possible confusion, the cost of electricity used to charge PHES, whether from the renewable energy sources or a natural grid, was neglected because it was only necessary to calculate the energy loss variation between the proposed specific pipe diameter and the large pipe diameter

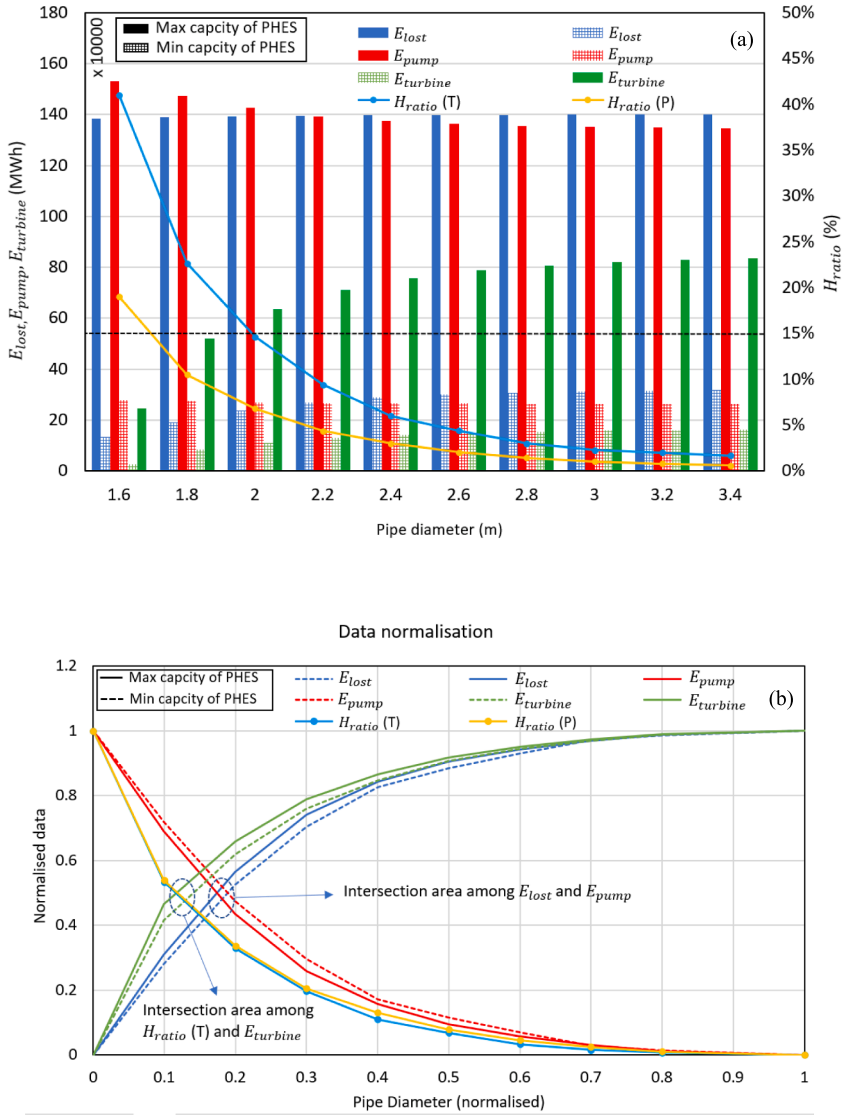

Fig. 10. H_{ratio} for each possible pipe diameter and total energy: (a) actual data (b) data normalisation.

Table 2
Average monthly meteorological data.

Month	Temperature (°C)	Load (MW)	Solar radiation (W/m^2)	Wind speed (m/s)
January	16.4	244.9	228.4	2.8
February	20.0	241.1	264.6	3.3
March	22.7	237.8	301.5	3.6
April	24.5	254.9	281.2	2.9
May	28.4	313.6	290.3	3.2
June	31.1	364.3	310.4	3.5
July	30.8	362.1	293.1	4.6
August	30.7	355.9	301.6	3.7
September	29.3	313.1	301.5	3.7
October	24.2	249.5	253.0	3.5
November	21.8	232.7	210.9	3.4
December	19.3	227.2	215.4	3.3

3.4 m. Next, C_{pipe} and $C_{E,loss}$ for all the proposed pipe dimeters were calculated for a lifetime of 10 years [26], and E_{cost} was assumed to be 0.08 $/kWh, which is approximately the minimum price at which electricity might be sold, as proposed by [29]. Fig. 11 shows that C_{pipe} increases while $C_{E,loss}$ decreases because the small pipe diameter is associated with high H_{loss}, leading to more energy being lost than would have been sold. The grey bar refers to variations in the two variables at each proposed diameter, as C_{pipe} is subtracted from $C_{E,loss}$. It is shown that pipe diameters between 1.6 and 2 m have positive total cost values. After this point, the variation becomes negative because C_{pipe} is larger than $C_{E,loss}$ at the corresponding pipe dimeter, which means that the system would make a higher profit with less H_{loss} and would have to pay extra for an increased pipe diameter.

4.2.3. Optimal pipe diameter

Significantly, the pipe diameter of 2 m satisfies the proposed study conditions (two technical conditions proposed in 2.2.1) as presented by the black dash line in Fig. 10-(a). Also, from Fig. 10-(b), it is evident that this pipe diameter is a perfect selection as the intersection between all the intended variables for the maximum and minimum capacity of PHES occurring before this specific diameter. Furthermore, this pipe diameter is economically optimal and close to the point where the two variables of C_{pipe} and $C_{E,loss}$ intersect, as presented in Fig. 11. It was concluded that the 2 m pipe was the right choice from the technical and economic perspectives.

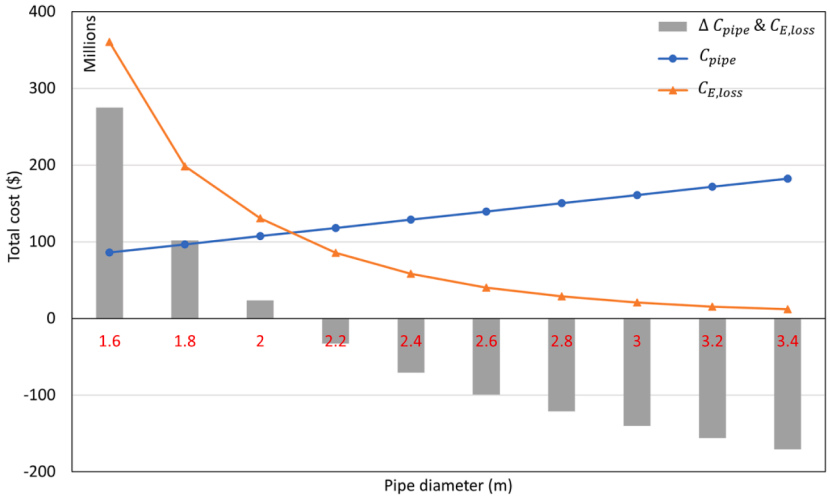

$C_{pipe}C_{E,loss}$

Fig. 11. Economic optimisation between C_{pipe} and $C_{E,loss}$ and variation in the two costs.

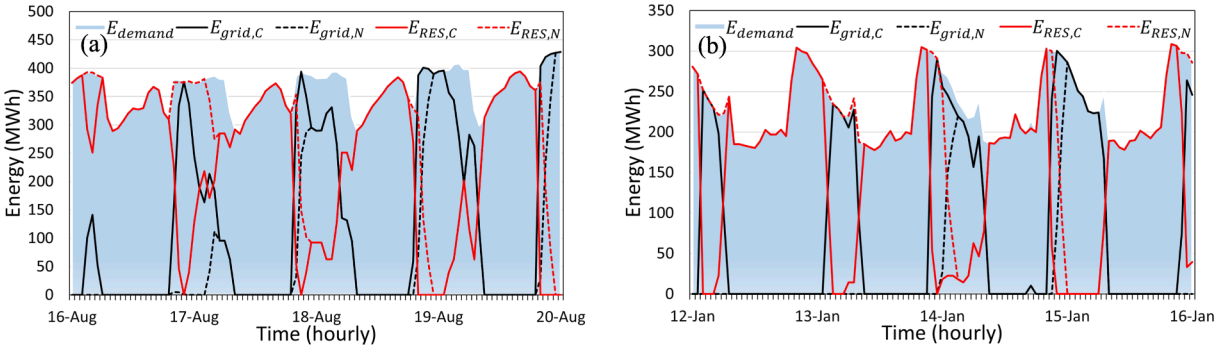

Fig. 12. The variation of E_{grid} and E_{RES} for four days in (a) summer and (b) winter.

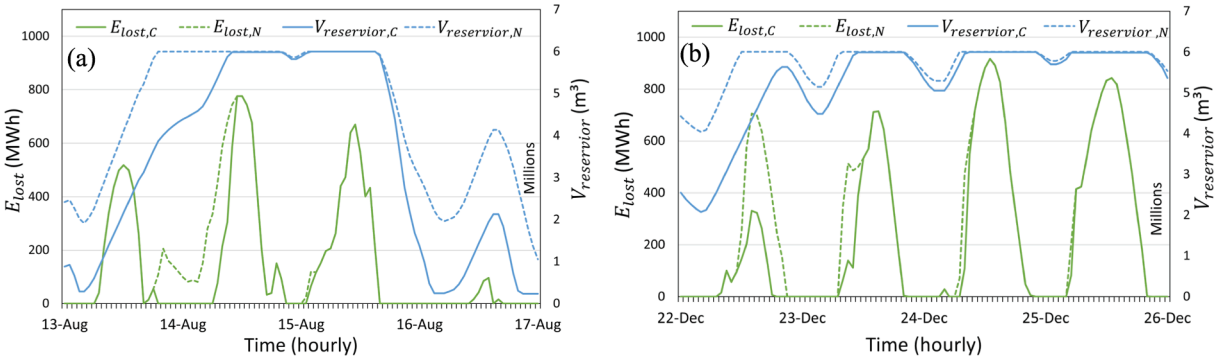

Fig. 13. The variation of E_{lost} and $V_{reservior}$ for four days in (a) summer and (b) winter.

4.3. Performance characteristics of HRES

After a specific pipe diameter has been selected and its regression equations to predict the actual H_{loss} are provided, the investigation of the short- and long-term impacts on the HRES performance is conducted. This investigation is performed by focusing on the comparison between considering (C) and neglecting (N) H_{loss} factor in terms of the HRES performance indicators *REF*,*LORE*, E_{RES}, and E_{lost}. It should be noted that the variable E_{RES} includes $E_{turbine}$ for analysis simplification as the PHES exploits E_{excess} to pump water without considering the off-peak national grid energy, and E_{lost} might be sold to the National Grid or abandoned, and it needs to be as low as possible as it is supposed to be dumped as considered in this study.

4.3.1. Short term analysis

Only one random configuration has been applied in this section, and the specifications of the configuration variables (N_{solar}, N_{wind}, $N_{P/T}$, V_{res}) are 1 GW, 1.1 GW, 5 pumps/turbines, and 6 Mm^3, respectively. Four days in two different seasons (summer, winter) have been selected as a sample of days in the hot and cold periods in which the amount of E_{demand}

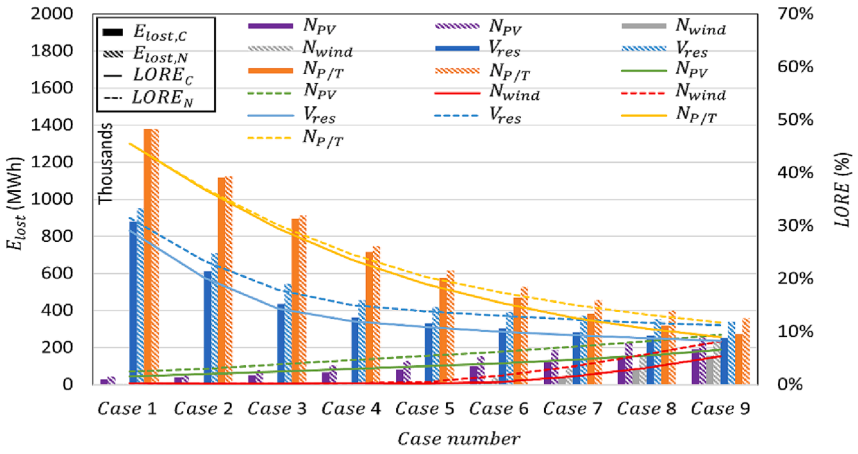

Fig. 14. E_{lost} and *LORE* in terms of all the proposed configurations (both scenarios, C and N).

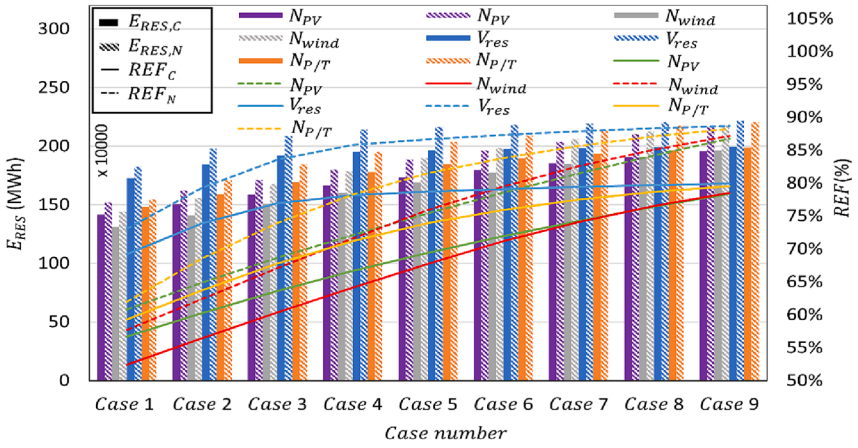

Fig. 15. The E_{RES} and *REF* in terms of all the proposed configurations (both scenarios, C and N).

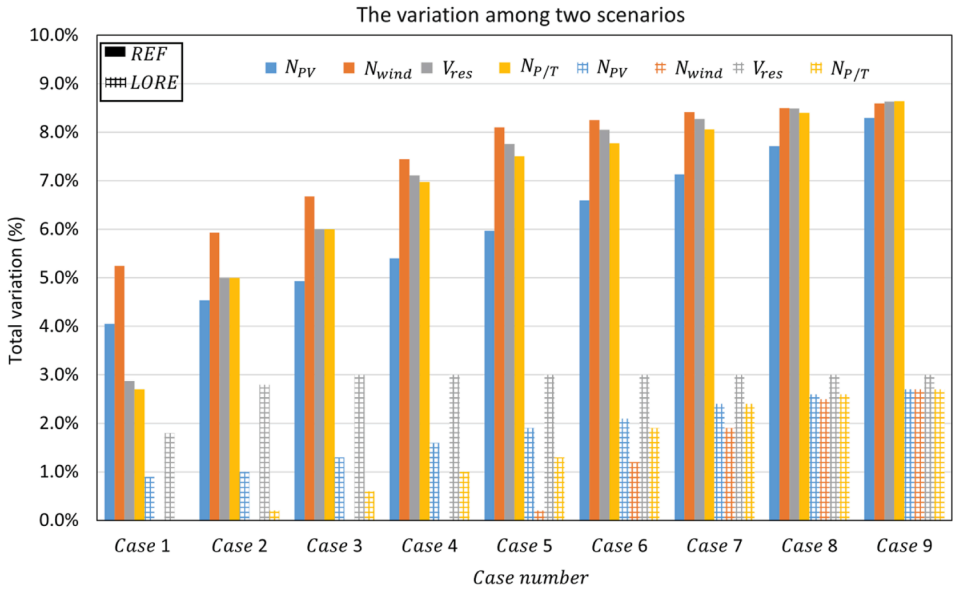

Fig. 16. The variation between neglected and considered H_{loss} in simulation tool.

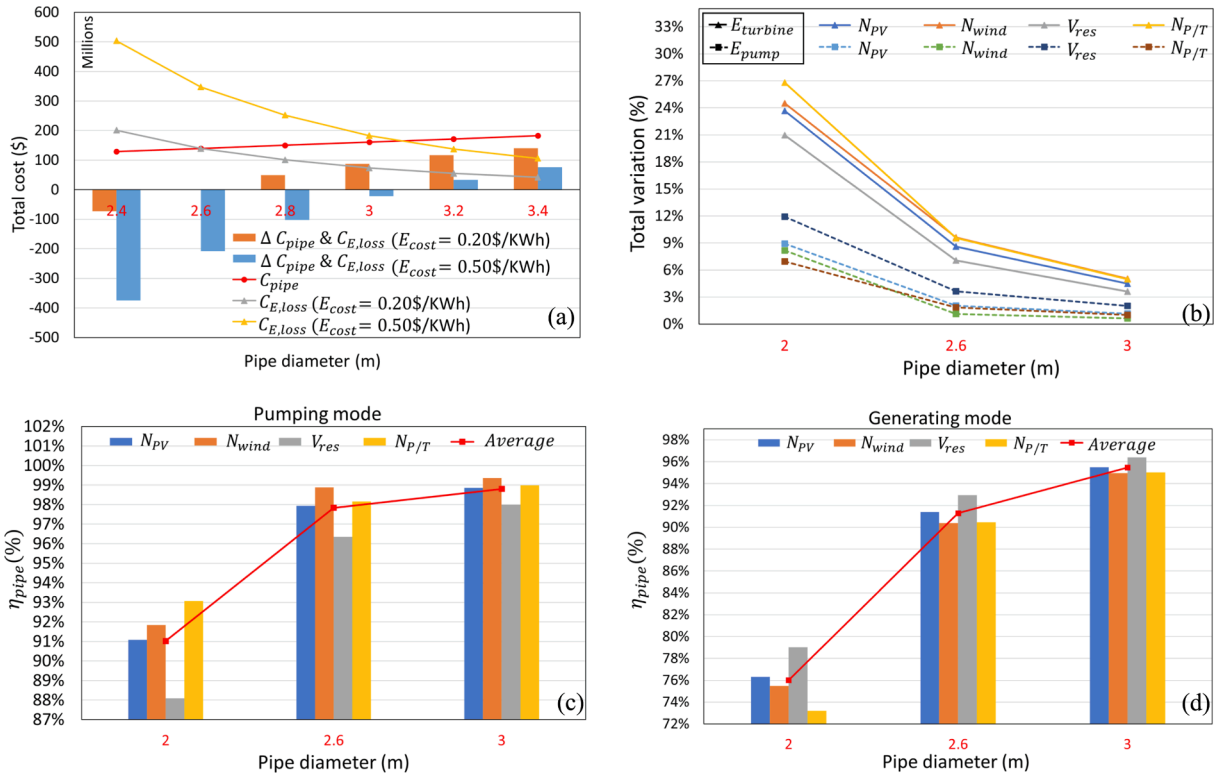

Fig. 17. (a) Economic optimisation between C_{pipe} and $C_{E,loss}$ for different electricity prices, (b) the total variation of E_{pump} and $E_{turbine}$ for three different pipe diameters and (c,d) average pipe efficiency for the pumping and generating modes.

Table A1
Photovoltaic electrical characteristics of KC200GT [33].

Parameter	Value	Unit
Max Power	200	[W]
Max Power Voltage	26.3	[V]
Max Power Current	7.61	[A]
Open Circuit Voltage	32.9	[V]
Short Circuit Current	8.21	[A]
Max System Voltage	600	[V]
Temperature Coefficient of V_{oc}	-1.23×10^{-1}	[V/°C]
Temperature Coefficient of I_{sc}	3.18×10^{3}	[A/°C]

Table A2
Wind turbine technical specifications of Gamesa G114-2 MW[35].

Parameter	Value	Unit
Rated power	2	[MW]
Cut-in speed	2.5	[m/s]
Rated wind speed	10	[m/s]
Cut-out speed	25	[m/s]
Swept area	10,207	[m^2]
Hub height	120	[m]

Table A3a
PHES mathematical model equations [2,20].

PHES	Equations	
Pumping mode	$Q_P = \frac{P_P \eta_{pu} N_{Pump}}{\rho_{water} g H_{total}}, where H_{total} = H_{st} + H_{pu}$	(A.11)
Generating mode	$P_T = Q_T H_{total} \rho_{water} g \eta_{tU} N_{turbine}, H_{total} = H_{st} - H_{tu}$	(A.12)
Static and head loss	$H_{pu}, H_{tu} = K\frac{V_f^2}{2g}, where V_f = \frac{Q}{0.25\pi d^2}$	(A.13)
	$K = K_{pipe} + K_{fittings}, where K_{pipe} = \frac{fL}{d}$	(A.14)
	$f = \frac{0.25}{\log\left(\left(\frac{\varepsilon}{3.7d}\right) + \left(\frac{5.74}{Re^{0.9}}\right)\right)^2}, where Re = \frac{\rho_{water} V_f d}{\mu}$	(A.15)
	$H_{st} = H_v + H_{lup}, where H_{lup} = \frac{V_{reservior}}{V_{res}} \times H_{up}$	(A.16)
Upper and lower reservior	$V_{reservior} = (Q_P - Q_T - V_e)^* t, where V_e = \frac{ET}{3.6^*10^6} A_{res} \times t$	(A.17)
Evaporation rate	$ET = \frac{0.408 S_v (G_t - S_{he}) + \left(\gamma^* \left(\frac{37}{T_{hr}+273}\right)\right)^* u_z \left(e^0(T_{hr}) - e_a\right)}{S_v + \gamma(1 + 0.34 u_z)}$	(A.18)

is entirely unequal (Fig. 6). So, E_{grid} and E_{RES} are shown with E_{demand}, as presented in Fig. 12-(a) for summer and (b) for winter. Clearly, when there is E_{lost}, there is no E_{grid}, and then at the same time, there is no difference shown between the two scenarios (C and N). Since the variation between the two scenarios is only shown when the PHES operates, it shows that having more E_{grid} increases the variation between the two scenarios; because of that E_{demand} starts to be covered by the National Grid once all the water volume stored in the upper reservoir has been released. Then, it is noted that there is a remarkable difference between $E_{grid,C}$ and $E_{grid,N}$ in the hourly simulation results. Particularly, $E_{grid,C}$ is higher than in the other scenario for all days due to H_{loss}, which is more accurate than $E_{grid,N}$. Also, the gap between the two scenarios in Summer is less than that in Winter because there are more E_{RES} in the Summer while the PHES is more frequently used in periods of electrical shortage. From the same figure, it also shows that $E_{REF,N}$ is greater than $E_{REF,C}$ for the two different periods, clearly having impacts of considering H_{loss}. In addition, it could be realised that during the daytime in the winter period, E_{RES} increases, as well as E_{demand} increasing and then when it gets darker, E_{RES} starts to decrease with the fact that the variation between

Table A3b
PHES components information.

Parameters	Value	Unit
Static head	350	[m]
Pump efficiency	80	[%]
Generator efficiency	80	[%]
Length of penstock	3800	[m]
Fitting resistance coefficient	10	[-]
Upper reservoir height	20	[m]
Maximum amount of P_T, P_P	75	[MW]
Minimum amount of P_P, P_T	40	[MW]
Maximum flow velocity $V_{f,max}$	10	[m/s]
Maximum head loss ratio H_{ratio}	15	[%]

the two scenarios becomes more obvious due to PHES being operated to satisfy the demand.

Fig. 13-(a,b) presents the volume of the upper reservoir ($V_{reservior}$) and $E_{turbine}$ in two different seasons. It can be seen that when there is a variation between $V_{reservior,C}$ and $V_{reservior,N}$, E_{lost} becomes clearer, but when the upper reservoir is full, there is no gap between the two scenarios. In addition, the difference of each day is different from any other because of the variation in $E_{pv+wind}$ as well as the availability of $V_{reservior}$ every day. It is concluded that the variation among the two scenarios shows up in the entire system performance when PHES starts operating because of the direct relationship between the two intended parameters with the components of PHES.

4.3.2. Long term analysis

With regard to the long-term assessment, the simulation performance of HRES for all the proposed configurations has been accomplished by taking the sum of E_{RES}, E_{lost}, *LORE*, and *REF* over 8760 h. Fig. 14 presents the amount of E_{lost} and *LORE* for both the scenarios (C and N) for thirty-six proposed configurations. It should be noted that, in both the scenarios, E_{lost} and for the two variables N_{pv} and N_{wind} start increasing by different amounts until they reach $Case_9$ with the value of 271.423 GWh and 236.821 GWh for the neglected scenario (N) and 189.770 GWh and 154.703 GWh for the considered scenarios (C), respectively. This is because of the fact that increasing capacity of the main power source (PV + wind turbine) covers more electricity demand during the peak period but in the case of low demand, the generated energy would be lost. In contrast, for both the scenarios, E_{lost} for V_{res} and $N_{P/T}$ decreases slightly from $Case_1$ until $Case_9$ with the value of 339.393 GWh and 356.371 GWh for the neglected scenarios and 250.002 GWh and 271.693 GWh for the considered scenario, respectively. This is because of the fact that increasing capacity of V_{res} and $N_{P/T}$ decreases the amount of E_{lost}. It can also be seen that the variation between all the variables becomes more apparent with an increase in the case number, and the total $E_{lost,N}$ for all the thirty-six configurations is greater than for $E_{lost,C}$. This is because, in the case of neglected scenarios, in the charging period, the water volume of the upper reservoir is determined as full earlier than the considered scenarios as a result of neglecting H_{loss}. The highest point of $LORE_N$ and $LORE_C$ occurs with $N_{P/T}$ with the value of 46% and therefore, no variation between the two scenarios occurs because of the small pump/turbine capacity at $Case_1$. In addition, N_{wind} starts increasing from $Case_6$ for both the scenarios, and because of that most of the wind energy is utilised whether for direct demand or pump water depending on the variations in the strength of the wind throughout the day.

With regard to the second study performance *REF* and E_{REF} for the thirty-six configurations, the most significant values of $E_{REF,C}$ and $E_{REF,N}$ occurs with V_{res} at (1.997, 2.215) TWh, and their REF_C and REF_N are 80%, and 88.6%, respectively, as presented in Fig. 15. However, in the same figure, it can be seen that the lowest points of $E_{REF,C}$ and REF_C happen with N_{wind}, in $Case_1$ with the value of 1.309 TWh and 52%, respectively. It can also be seen that all the variables increase gradually from $Case_1$ to $Case_9$ except V_{res} which remains mostly at the same level from $Case_5$ until reaching $Case_9$. This is because increasing V_{res} leads to the storing of more potential energy based on the availability of E_{excess} and more unused space is provided. Eventually, regarding the variation between the two scenarios in terms of E_{REF} and E_{lost} , the most influential variable is V_{res}, with a value of 218.23 GWh and 89.39 GWh, respectively.

4.3.3. Variation between the two scenarios

Fig. 16 summarises the actual variation in percentage between the two scenarios for all the variables in all the cases studied. It can be seen that the total variation with the variable of N_{wind} varies significantly from $Case_1$ to $Case_5$ and then starts raising gradually until $Case_{10}$. This is because when N_{wind} capacity increases, the electricity demand is mainly met by direct wind power, then there is less variation after this point because of lower use of the PHES system. In addition, from the same figure, it is clear that the most significant variation occurs at 8.6 % regarding *REF*, occurring with three variables of N_{wind}, $N_{P/T}$, V_{res}. With regard to *LORE* it can be seen that the variable V_{res} increases from $Case_1$ with a value of 2 % to $Case_3$, and then remains with the same variation until $Case_3$ with a value of 3 %. In addition, the variables of $N_{pv,}$ N_{wind} and $N_{P/T}$ start increasing with values of 1 %, 0 %, and 0 % until they reach $Case_9$ with values of 3 %, respectively. Significantly, these results emphasise that the *REF* and *LORE* indicators are influenced more by varying the large capacity of renewable sources and increasing the PHES capacity to the entire system. It is worth considering that this study increases the prediction accuracy by 11.6 % which is the sum amount of large error for *REF* and *LORE*.

4.4. Sensitivity analysis

E_{cost} is the most significant parameter for selecting the most economical pipe diameter, and it varies based on the factors such as the specific location and type of energy sources utilised. Therefore, this section comprehensively assesses the different economic pipe diameters based on the variations in E_{cost}. The reason behind conducting this sensitivity analysis was to determine the pipe efficiency (η_{pipe}) without conducting the entire analysis by relying only on E_{cost} under the proposed study boundaries. The E_{cost} of 0.08 $/kWh was already assessed, and a pipe diameter of 2 m was chosen as the most economical design, as already described in Fig. 11. This is considered as a small E_{cost}; thus, both the average and high E_{cost} globally were proposed to be 0.2 and 0.5 $/kWh, respectively [30]. Fig. 17-(a) shows the optimal pipe diameter for the E_{cost} of 0.20 and 0.50 $/kWh, which are 2.6 m and 3 m, respectively. This is because increasing C_{pipe} with a high E_{cost} led to an increase in the total $C_{E,loss}$. As each pipe diameter was selected by relying on a different E_{cost}, only the total variation between the two proposed scenarios (C/N H_{loss}) for E_{pump} and $E_{turbine}$ was assessed to calculate an accurate η_{pipe} for each proposed E_{cost}. Due to simplification, the average results of all the 10 proposed cases for each variable of N_{PV}, N_{wind}, V_{res} and $N_{P/T}$ were determined, as explained in section 2.3 . Fig. 17-(b) shows the total variation between the mentioned scenarios of pipe diameters of 2 m, 2.6 m and 3 m, respectively. The largest variation occurred with variables V_{res} and $N_{P/T}$ for E_{pump} and $E_{turbine}$, with the values of 12 % and 27 %, respectively. The reason behind this was that a large reservoir would increase the number of pumping cycles, and increasing $N_{P/T}$ raises the use of $E_{turbine}$, resulting in increased H_{loss}. Based on all the variations' values, total η_{pipe} was calculated for the pumping and generating modes for the three different pipe diameters for all the 10 cases, relying on the three different E_{cost}. Fig. 17(c–d) further shows that the average η_{pipe} in the pumping mode resulted in 91 %, 98 % and 99 % for the pipe diameters of 2 m, 2.6 m and 3 m, respectively. For the generating mode, however, the average η_{pipe} was 76 %, 91 % and 95 % for the pipe diameters of 2 m, 2.6 m and 3 m, respectively. Eventually, any value within the range of the average efficiency might initially be

assumed when calculating the power required to pump a specific quantity of water or cover a certain amount of energy with a turbine. This implies that, during the early stage of design, real implementation of PHES with the same specifications used in this study, and these numbers could be added to the overall efficiency with a reasonable certainty and without the need to undertake the entire analysis conducted already. The average efficiency values suggested in this section, whether for the pumping or generation modes, are based on a detailed technical and economic analysis that takes into account the diversity in the pipe design and cost of energy.

5. Conclusions

To precisely design the proposed HRES, the mathematical model of each subsystem (PV, wind and PHES) requires the consideration of many critical indexed parameters. In contrast, neglecting or misestimating these essential parameters in the simulation performance process leads to over- or underdetermining each subsystem's accurate size. Thus, the H_{loss} occurring inside the pipe and evaporation rate from the upper reservoir of PHES are the essential factors, particularly when related to the areas with dry climates and no continuous inflows of water, such as Saudi Arabia. The present work has considered these two factors in the simulation performance of the entire HRES operation. In addition, an efficient approach and strategy for identifying the optimal pipe design through a comprehensive techno-economic analysis were developed with the intent of boosting the precision of the overall system design results. The comparative model was applied between the two scenarios, one of which considered the H_{loss} and one that did not. Up to 36 design configurations involving variations of N_{pv}, N_{wind} , V_{res} and $N_{P/T}$ were assessed. The *REF* and *LORE* were applied as the main performance indicators for designing the proposed HRES. The results further revealed that the total variation of *REF* and *LORE* was 8.6% and 3%, respectively. Furthermore, the most significant annual variation between the two scenarios regarding E_{REF} and E_{lost} appears with the design variable of V_{res} reaching 218.23 GWh and 89.39 GWh, respectively. A sensitive analysis based on the different energy costs worldwide showed variations of η_{pipe} for the pumping and generating modes, ranging between 91 and 99% and 76–95%, respectively. Regarding the monthly evaporated water, the highest and lowest points were found to occur in the months of July and August, with the values of 338 mm and 169 mm, respectively. In addition, the total amount of evaporated water in one year was 3042 mm, which is a remarkable value for a closed-loop PHES. Therefore, the results have shown that the H_{loss} and evaporation rate should be considered in the PHES mathematical model to avoid uncertainty in the simulation outcomes. This uncertainty may result in undesired effects with the consequences of over- or undersizing renewable energy sources and the PHES, or a mismatch between the energy supplied and derived in the operation strategy process. Eventually, further investigation outside the scope of this research could be conducted. This includes the impact of weather data uncertainty on the design of a particular pipe and the investigation of the downsizing of HRES and PHES.

CRediT authorship contribution statement

Bader Alqahtani: Conceptualization, Methodology, Software, Validation, Investigation, Formal analysis, Visualization, Writing – original draft, Writing – review & editing. **Jin Yang:** Supervision, Writing – review & editing. **Manosh C Paul:** Conceptualization, Supervision, Writing – review & editing, Project administration.

Declaration of Competing Interest

The authors declare that they have no known competing financial interests or personal relationships that could have appeared to influence the work reported in this paper.

Data availability

Data will be made available on request.

Acknowledgements

The authors are thankful to the Deanship of Scientific Research at University of Bisha for supporting this work through the Fast-Track Research Support Program.

Appendix A

In this section, a mathematical model of each component linked to the proposed hybrid system is presented, along with any assumptions made.

A.1 Photovoltaic model

All equations on which the method relies to calculate electricity produced from PV are expressed below [31,32]:

$$P_{pv} = (I \times V) \times PR \times N_{pv} \tag{A.1}$$

$$I = I_{pv} - I_0\left[Exp\left(\frac{V + R_s I}{V_t a}\right) - 1\right] - \frac{V + R_s}{R_p} \tag{A.2}$$

$$I_{pv} = \left(I_{pv,n} + K_I \Delta T\right) \times \left(\frac{G}{G_n}\right) \tag{A.3}$$

$$I_0 = (I_{sc,no} + K_I \Delta T)/[Exp\left(\frac{\left(V_{oc,noc} + K_v \Delta T\right)}{aV_t}\right) - 1] \tag{A.4}$$

$$V_t = \frac{N_s kT}{q} \tag{A.5}$$

$$P_{max,cal} = V_{mp}\left(I_{pv} - I_0\left(\exp\left(\frac{q}{kT} \times \frac{V_{mp} + R_s I_{mp}}{aN_s}\right) - 1\right) - \frac{V_{mp} + R_s I_{mp}}{R_p}\right) = P_{max,exp} \tag{A.6}$$

$$R_p = \frac{V_{mp}\left(V_{mp} + I_{mp} \times R_s\right)}{\left\{V_{mp}I_{pv} - V_{mp}I_0 \times Exp\left(\begin{array}{c}(V_{mp} + I_{mp} \times R_s/(N_s \times a))\\ \times\left(\frac{q}{KT}\right)\end{array}\right) + \left(V_{mp}I_0\right) - P_{max,exp}\right\}} \quad (A.7)$$

$$T = T_a + \left(T_{noc} - T_{a,noc}\right)\left(\frac{G_t}{G_{noc}}\right)\left(\frac{U_{L,noc}}{U_L}\right)\left(1 - \frac{\eta_c}{\alpha\tau}\right) \quad (A.8)$$

(See Table A1*)*

A.2 Wind turbine model

The wind turbine power production is calculated as follows [34]:

$$P_{wind}(v) = \frac{1}{2}\rho_{air}A_{bl}C_p v^3 \eta_{wg} N_{wind} \quad (A.9)$$

The wind speed at hub elevation is calculated on the basis of the wind speed measured at the ground level, as expressed below:

$$v = v_1(Elv/Elv1)^{\alpha} \quad (A.10)$$

(See Table A2.)

A.3 Pumped hydropower energy storage model

The mathematical model of PHES is presented in Table A3a., and all technical specification assumption for PHES is shown in Table A3b..

A.4 Integrated system energy balance

The HRES includes various energy sources as well as primary energy storage. First, each sub-system is individually modelled, and then they are all interfaced using the proposed operating strategy that consists of connected steps starting with desired inputs and then following the orders with constraints, as explained earlier. Then, the dynamic behaviour of the proposed system based on the flow chart in Fig. 5 is conducted to further validate the results, and energy balance has been performed as presented below:

$$\sum_{t=1}^{t_{end}} E_{pv} + E_{wind} + E_{grid} + E_{turbine} = \sum_{t=1}^{t_{end}} E_{demand} + E_{pump} + E_{lost} \quad (A.19)$$

References

[1] Aneke M, Wang M. Energy storage technologies and real life applications – A state of the art review. Appl Energy 2016;179:350–77. https://doi.org/10.1016/j.apenergy.2016.06.097.

[2] Mousavi N, Kothapalli G, Habibi D, Khiadani M, Das CK. An improved mathematical model for a pumped hydro storage system considering electrical, mechanical, and hydraulic losses. Appl Energy 2019;247:228–36. https://doi.org/10.1016/j.apenergy.2019.03.015.

[3] Jurasz J, Mikulik J, Krzywda M, Ciapała B, Janowski M. Integrating a wind- and solar-powered hybrid to the power system by coupling it with a hydroelectric power station with pumping installation. Energy 2018;144:549–63. https://doi.org/10.1016/j.energy.2017.12.011.

[4] Singh P, Pandit M, Srivastava L. "Multi-objective optimal sizing of hybrid micro-grid system using an integrated intelligent technique,". Energy 2023;269 (November 2022):126756. https://doi.org/10.1016/j.energy.2023.126756.

[5] Poonam S, Manjaree P, Laxmi S. Comparison of traditional and swarm intelligence based techniques for optimization of hybrid renewable energy system. Renew Energy Focus 2020;35(December):1–9. https://doi.org/10.1016/j.ref.2020.06.010.

[6] Nassar YF, et al. Dynamic analysis and sizing optimization of a pumped hydroelectric storage-integrated hybrid PV/Wind system: A case study. Energy Convers Manag 2020;229(September 2021):113744. https://doi.org/10.1016/j.enconman.2020.113744.

[7] Jurasz J. Modeling and forecasting energy flow between national power grid and a solar–wind–pumped-hydroelectricity (PV–WT–PSH) energy source. Energy Convers Manag 2017;136:382–94. https://doi.org/10.1016/j.enconman.2017.01.032.

[8] Ma T, Yang H, Lu L. Feasibility study and economic analysis of pumped hydro storage and battery storage for a renewable energy powered island. Energy Convers Manag Mar. 2014;79:387–97. https://doi.org/10.1016/j.enconman.2013.12.047.

[9] Guezgouz M, Jurasz J, Bekkouche B, Ma T, Javed MS, Kies A. Optimal hybrid pumped hydro-battery storage scheme for off-grid renewable energy systems. Energy Convers Manag 2019;199(May):112046. https://doi.org/10.1016/j.enconman.2019.112046.

[10] Ma T, Javed MS. Integrated sizing of hybrid PV-wind-battery system for remote island considering the saturation of each renewable energy resource. Energy Convers Manag 2018;182(December 2019):178–90. https://doi.org/10.1016/j.enconman.2018.12.059.

[11] Portero U, Velázquez S, Carta JA. Sizing of a wind-hydro system using a reversible hydraulic facility with seawater. A case study in the Canary Islands. Energy Convers Manag 2015;106:1251–63. https://doi.org/10.1016/j.enconman.2015.10.054.

[12] Pali BS, Vadhera S. A novel pumped hydro-energy storage scheme with wind energy for power generation at constant voltage in rural areas. Renew Energy 2018;127:802–10. https://doi.org/10.1016/j.renene.2018.05.028.

[13] Ming B, Liu P, Cheng L, Zhou Y, Wang X. Optimal daily generation scheduling of large hydro–photovoltaic hybrid power plants. Energy Convers Manag 2018;171 (April):528–40. https://doi.org/10.1016/j.enconman.2018.06.001.

[14] "Population, total - Saudi Arabia | Data." https://data.worldbank.org/indicator/SP.POP.TOTL?locations=SA (accessed Mar. 24, 2021).

[15] "Saudi Arabia's Vision 2030: Key electric power decisions ahead - Atlantic Council." https://www.atlanticcouncil.org/blogs/energysource/saudi-arabia-s-vision-2030-key-electric-power-decisions-ahead/ (accessed Mar. 25, 2021).

[16] "The plan to turn Saudi Arabia into a renewable energy leader | Saudi Arabia 2019 | Oxford Business Group." https://oxfordbusinessgroup.com/news/plan-turn-saudi-arabia-renewable-energy-leader (accessed Mar. 25, 2021).

[17] Obaid RR. Seasonal-water dams: A great potential for hydropower generation in saudi arabia. Int J Sustain Water Environ Syst 2015;7(1):1–7. https://doi.org/10.5383/swes.7.01.001.

[18] K. Kotiuga, W., Hadjian, S., King, M., Al-Hadhrami, L., Arif, M., Khaled, Y. and Al-Soufi, "Pre-Feasibility Study of a 1000 MW Pumped Storage Plant in Saudi Arabia," no. July, 2013.

[19] S. Rehman, L. M. Al-Hadhrami, and M. M. Alam, "Pumped hydro energy storage system: A technological review," *Renewable and Sustainable Energy Reviews*, vol. 44. Elsevier Ltd, pp. 586–598, Apr. 01, 2015, doi: 10.1016/j.rser.2014.12.040.

[20] Al-Garalleh AA. Design of a pumped hydroelectric energy storage system for Jordan. The unversity of Jordan 2017.

[21] E. Power and D. Co, "Data Collection Survey on Pumped Storage Hydropower Development in Maharashtra Final Report October 2012 Japan International Cooperation Agency," no. October, 2012.

[22] L. A, "A dimensional analysis for determining optimal discharge and penstock diameter in impulse and reaction water turbines A dimensional analysis for determining opti- mal discharge and penstock diameter in im- pulse and reaction

water turbines Introduction," pp. 609–615, 2014, doi: 10.1016/j.renene.2014.06.024.
[23] "Pipe Head Loss." https://www.homerenergy.com/products/pro/docs/latest/pipe_head_loss.html (accessed Jul. 31, 2022).
[24] Jha NK. Graphical approach in optimization of penstock diameter. Int Res J Innov Eng Technol 2020;4(8):25–30. https://doi.org/10.47001/irjiet/2020.408005.
[25] et al. AWWA, Staff, : A guide for design and installation . American Water Works Association. 2004.
[26] Shabani M, Dahlquist E, Wallin F, Yan J. Techno-economic comparison of optimal design of renewable-battery storage and renewable micro pumped hydro storage power supply systems: A case study in Sweden. Appl Energy 2020;279(August):115830. https://doi.org/10.1016/j.apenergy.2020.115830.
[27] "NSRDB." https://nsrdb.nrel.gov/ (accessed Mar. 10, 2022).
[28] "Saudi Electricity Company." https://www.se.com.sa/en-us/Pages/home.aspx (accessed Mar. 10, 2022).
[29] Smallbone A, Jülch V, Wardle R, Roskilly AP. Levelised cost of storage for pumped heat energy storage in comparison with other energy storage technologies. Energy Convers Manag 2017;152(September):221–8. https://doi.org/10.1016/j.enconman.2017.09.047.
[30] "Electricity prices around the world | GlobalPetrolPrices.com." https://www.globalpetrolprices.com/electricity_prices/ (accessed Feb. 08, 2023).
[31] Villalva MG, Gazoli JR, Filho ER. Comprehensive approach to modeling and simulation of photovoltaic arrays. IEEE Trans Power Electron 2009;24(5):1198–208. https://doi.org/10.1109/TPEL.2009.2013862.
[32] Li W, et al. A scaling law for monocrystalline PV/T modules with CCPC and comparison with triple junction PV cells. Appl Energy 2017;202:755–71. https://doi.org/10.1016/j.apenergy.2017.05.182.
[33] Multicrystal HE, Module P, Trends MG, Kong H. "Highlights of" 2009.
[34] Manwell JF, McGowan JG. Wind energy explained theory. Design and Application Second Edition 2009.
[35] "Gamesa G114-2.0MW - 2,00 MW - Wind turbine." https://en.wind-turbine-models.com/turbines/428-gamesa-g114-2.0mw (accessed Mar. 30, 2021).